CORE
Metadata, citation and similar papers at core.ac.uk
Provided by NASA Technical Reports Server

Reprinted from JOURNAL OF THE ATMOSPHERIC SCIENCES, Vol. 52, No. 10, 15 May 1995
American Meteorological Society

Computation of Vertical Profiles of Longwave Radiative Cooling over the Equatorial Pacific

PERRY G. RAMSEY AND DAYTON G. VINCENT

Department of Earth and Atmospheric Sciences, Purdue University, West Lafayette, Indiana

(Manuscript received 18 February 1994, in final form 29 August 1994)

ABSTRACT

An important quantity whose magnitude has not been thoroughly examined is the vertical distribution of heating in the Tropics. The details of the vertical distribution of heating have a significant impact on a number of phenomena, including the 30–60 day oscillation, sometimes known as the intraseasonal oscillation. Prior attempts to establish the structure of the heating relied on limited field data or assimilated data, coupled with climatological radiative heating parameters. The availability of high quality global-scale datasets has made it possible to make more accurate calculations than were possible a few years ago.

An important component of the apparent heat budget is the longwave radiative cooling, which in this paper is found by using the ECMWF/WCRP/TOGA Archive II and ISCCP C1 datasets, together with a well-established parameterization scheme. A method is developed that can be used to estimate the vertical structure of cloud amounts based on top-of-atmosphere cloud observations, and the results are used with a wide-band longwave parameterization to produce longwave cooling rates over the tropical Pacific Ocean.

Outgoing longwave radiation is calculated and compared to ERBE results. The calculated values are generally higher than those from ERBE, though the spatial distributions are similar. Some significant problems exist with the ECMWF upper-tropospheric water vapor amounts, which could imply uncertainties of 0.5°C day $^{-1}$ in the calculated cooling rates. This is comparable to the differences associated with the minimum or random overlap assumptions used to generate cloud profiles.

1. Introduction

The vertical distribution of diabatic heating is known to play an important role in the development and maintenance of atmospheric circulation systems on a variety of space and time scales. Within the Tropics, it is often the convective latent heating component of the diabatic heating that is most important, particularly for synoptic-scale systems that last several days. The problem is that vertical profiles of convective latent heat release either need to be parameterized or determined as residuals from some form of the thermodynamic equation. In the latter case, profiles of net radiation must be known, especially the longwave component. For the past 30 years, most researchers and numerical modelers have relied on a variety of convective parameterization schemes (e.g., Kuo 1965, 1974; Arakawa and Schubert 1974) (or some modification or combination of these schemes) to distribute the latent heat vertically. With the availability of new datasets, including those containing cloud information, it is now possible to attempt to derive radiation profiles, which, taken together with routine analyses, can be used to produce convective heating profiles. The primary purpose of this paper is to derive gridpoint profiles of longwave radiation over the "warm pool" region of the western Pacific where tropical convective systems frequently are initiated or enhanced.

The overall objective of this research is to combine the longwave profiles discussed here with shortwave radiation and dry static energy (Q_1) components (to be discussed in a companion paper) to produce vertical distributions of total convective heating (Yanai et al. 1973). The focus of the present paper is on regional space scales and monthly timescales, although the results could be applied to smaller spatial and temporal scales. The latter will be addressed in the companion paper. Because of uncertainties in many of the input quantities, a major focus of the paper is on examining the sensitivity of the longwave radiation results to the input errors.

Historically, climatological profiles of radiative heating have been used in Q_1-budget studies to represent shorter than climatological-scale processes. Later in this paper, we show that such profiles are not always representative of smaller-scale radiative distributions. In recent years, the direct calculation of short-term radiative components has become possible. M.-L. Wu and collaborators have produced all-sky results using HIRS2/MSU (Wu and Cheng 1989; Wu and Susskind 1990; and Wu and Chang 1992). Others have used an-

Corresponding author address: Dr. Dayton G. Vincent, Department of Earth and Atmospheric Sciences, Purdue University, 1397 Civil Engineering Building, West Lafayette, IN 47907-1397.

© 1995 American Meteorological Society

alyzed datasets to calculate clear-sky outgoing longwave radiation (OLR) (Kiehl and Briglieb 1992; Slingo and Webb 1992).

One of the datasets most widely used to represent the large-scale atmospheric state is produced by the European Centre for Medium-Range Weather Forecasts (ECMWF). The quality and quantity of observations and the assimilation techniques have improved markedly through the years, and these routinely produced analyses are readily available in archived format. Also, the International Satellite Cloud Climatology Project (ISCCP) (Schiffer and Rossow 1983) has created a global-scale cloud climatology. It is the objective of this paper to examine the feasibility of combining ECMWF analyses and ISCCP C1 data, together with a longwave radiative parameterization scheme to make accurate calculations of radiative cooling profiles. As noted above, an important part of this study is to test the sensitivity of the results to various parameters.

2. Analytical procedures

a. ECMWF dataset

The atmospheric state for this study is taken from the WCRP/TOGA Archive II version of the ECMWF global-scale upper-air analyses. A description and assessment of this dataset is given by Trenberth (1992). It contains uninitialized values of temperature, humidity, winds, and geopotential height at 10 tropospheric and 4 stratospheric levels. It also contains a record of surface temperature, 2-m air temperature, 2-m air dewpoint temperature, surface pressure, sea level pressure, and 10-m winds. All data are on a 2.5° × 2.5° lat–long grid.

b. Cloud dataset

Accurate representation of clouds has long been the most difficult problem in radiation calculations. The quality and quantity of observations have historically been inadequate for most applications. Because of the strong interactions between clouds and the radiation field, anything less than complete coverage with high vertical and horizontal resolution gives results of little usefulness.

Some studies rely on model-generated clouds in which a physical model is used to simulate temperature and humidity and clouds are generated through an empirical scheme based on physical parameters. The results are, unfortunately, highly dependent on the nature of the cloud parameterization, and observational studies show that modeled clouds are not highly correlated with the actual cloud distribution.

Recently, data from ISCCP have become available (Rossow et al. 1988). The principle behind ISCCP is to take radiances from imaging spacecraft (both geostationary and polar orbiting) and combine them with vertical temperature soundings from polar-orbiting spacecraft to detect and classify clouds. The ISCCP C1 dataset, used in this study, provides histograms of observed cloud amount on a 2.5° × 2.5° (approximate) equal area grid in seven pressure layers. A variety of information is available; for this study the most important data are the IR-only cloudiness statistics. The pressure level at the top of an observed cloud is determined by comparing the observed temperature with the atmospheric temperature given by TOVS (TIROS Operational Vertical Sounder). If the cloud is optically thick at IR wavelengths, this procedure produces reliable results, but optically thin clouds are not accurately represented. The IR-only cloudiness is normally available at all eight observing times throughout the day.

A second type of data available in ISCCP is the cloud-top pressure/visible optical depth distributions, often called the PC-TAU distributions. It is produced by comparing the IR-determined cloud-top pressure and the visible brightness. When visible information is available, it is used to check the assumption that the cloud is optically thick and adjustments can be made to the cloud height. The IR thickness is assumed to be proportional to the visible optical thickness, and the pixel-containing thin cloud is reanalyzed on that basis. Since visible data are available only during the daytime, these corrections can be made in no more than three of the eight daily observations. A scheme that uses this information to adjust the cloud field is discussed in section 2e.

Wu and Chang (1992) have used the ISCCP C1 data with satellite-derived temperature and humidity data to make longwave radiation calculations and Darnell et al. (1992) used them to make downward flux computations. These papers report top- and bottom-of-atmosphere results but do not report vertical distributions of cooling. Further, neither study includes adjustments for misidentification of thin cloud or for cloud overlap.

The ISCCP equal angle and ECMWF grids are both 2.5° × 2.5°, but the grid locations differ: the centers of the ISCCP equal angle grid correspond to the corners of the ECMWF archive grid. Since ISCCP cloud distributions represent discrete quantities, while the ECMWF data represent continuous fields, the ECMWF data were linearly interpolated to the ISCCP grid for this study.

c. ERBE

Cloudy- and clear-sky OLR ground truth data are taken from Earth Radiation Budget Experiment (ERBE). The ERBE data are based on active cavity radiometer observations. The data used in the project are from the GEDEX (Greenhouse Effect Detection Experiment) CD-ROM disk, obtained from National Space Science Data Center (NSSDC). Only the scanner data were used for this study. Scanner data are taken at an approximately 40-km resolution and merged into monthly averages on a 2.5° × 2.5° equal angle grid.

The ERBE cloudy-sky OLR is simply the summary of all observations taken through the 5–50-μm sensor. The ERBE clear-sky OLR is calculated from a summary of clear observations. The accuracy is reported by Harrison et al. (1990) to be ± 2 W m^{-2}, with a systematic bias of 4 W m^{-2}.

d. Derivation of layer-by-layer cloud amount using assumed overlap method

Since cloud tops are the only data available in ISCCP, some method for estimating the entire cloud structure must be used. Many authors (e.g., Gupta 1989) have assumed a constant thickness and no overlap. A more general assumption in estimating cloud amount is that clouds can be represented as some combination of maximally overlapping, minimally overlapping, and/or randomly overlapping clouds. The maximally overlapping cloud assumption implies that clouds are stacked vertically as much as possible. The minimally overlapping assumption means that clouds are not assumed to exist where they are not directly observed. The randomly overlapping assumption implies that clouds are randomly distributed throughout a scene so that there are clouds where they cannot be directly observed in proportion to their fraction where they are observed.

Though the maximum overlap assumption is commonly used in general circulation models to represent deep convective clouds, it is not a good way to estimate low clouds from satellite data. As demonstrated by Riehl (1979), cumulonimbus-type clouds cannot occupy more than a small fraction of the tropical belt. Maximum overlap would almost certainly lead to drastic overestimates of low clouds. The minimum overlap method considers only clouds that are directly observed and, therefore, forms a minimum boundary on any estimate of low cloud. Minimum overlap is tacitly employed by most researchers. In the case of randomly overlapping clouds it is assumed that the density of cloud is horizontally uniform throughout a layer, so that the fraction of randomly overlapping clouds present in obscured areas is the same as in unobscured areas. This provides a mechanism for generation of some low-level clouds beneath the cloud tops.

Consider the following numerical example. A satellite observes 25% cloudiness in a high layer and 25% cloudiness in a lower layer. This would be interpreted by the maximum overlap method to be 50% cloud in the lower layer, 25% by the minimum overlap method, and 33% by the random overlap method. Thus, some type of assumption or observations of the low cloud amount, is required to distinguish between these alternatives. If a closure assumption can be developed, it may be possible to develop a combined method that captures the best properties of more than one of the above methods.

Tian and Curry (1989), in a study using Real Time NEPH analysis (RTNEPH) data for the North Atlantic, compared total-cloudiness to cloud fractions generated with various overlap assumptions. Using the original 42-km grid, they concluded that the best representation of total cloud cover was derived when layers without intervening space were maximally overlapped and separated layers were randomly overlapped. Upon combining data from adjacent grid boxes into a reduced resolution dataset, the best results were found using the mean of the random and minimum overlap methods. They cautioned that this conclusion may be an artifact of the resolution reduction method. The applicability of their results to this study is also questionable because their observational domain is an area with considerable stratus cloud.

In this study, clouds will be estimated using a combination of the minimum and random overlap methods. By assuming that each layer can contain some minimally and some randomly overlapping clouds, the properties of each method can be combined to produce a method that will yield an intermediate estimate of cloudiness that is still consistent with the satellite observations. It must be acknowledged, however, that cumulonimbus with large, thick anvils represents a pathological case that cannot be adequately analyzed by this method. Warren et al. (1986) report an average amount of cumulonimbus in the region of interest of less than 10%, but this is recognized to be a significant overestimate due to reporting requirements. It is thus expected that the impact of ignoring cumulonimbus on long-term, large-scale averages will not be large.

In the following development, V_i represents the clear line of sight from space to the top of layer i, while M_i and R_i are the amount of minimally and randomly overlapping cloud, respectively, contained in layer i. The V_1 term is the view of the top of the atmosphere to space, so it is always 1. The V_2 term equals V_1 minus the fraction of layer 1 that contains clouds as seen by the satellite. Each subsequent V_{i+1} is found by subtract-

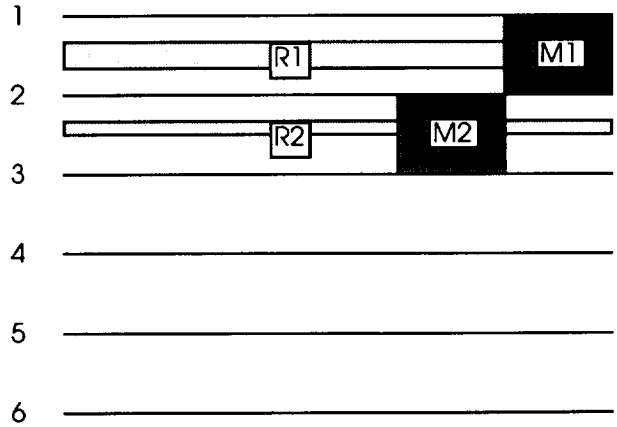

FIG. 1. Guide to estimation of low cloud amount using a combination of randomly and minimally overlapping clouds.

ing the directly observed cloud fraction of layer i from V_i. Referring to Fig. 1,

$$V_2 = (1 - M_1)\left(1 - \frac{R_1}{1 - M_1}\right). \quad (1)$$

The $(1 - M_1)$ term represents the portion of the level that does not contain minimally overlapping cloud, and $[1 - R_1/(1 - M_1)]$ represents the randomly overlapping clouds filling the remaining space that is cloudy. For layer 2 only, this reduces to $(1 - R_1 - M_1)$, the expected result for the total cloud amount in a single layer. Continuing in this manner,

$$V_3 = (1 - M_1 - M_2)\left(1 - \frac{R_1}{1 - M_1}\right)\left(1 - \frac{R_2}{1 - M_2}\right). \quad (2)$$

The minimally overlapping term has the form $(1 - M_1 - M_2)$ because each addition of minimally overlapping cloud excludes the possibility of a clear line of sight through that portion of the column. The randomly overlapping term has the form $[1 - R_1/(1 - M_1)][1 - R_2/(1 - M_2)]$ because it represents a reduction in the possibility of a clear line of sight. Carrying this process to the general limit, we find

$$V_{i+1} = [1 - (\sum_{j=1}^{i} M_j)] \prod_{j=1}^{i}\left(1 - \frac{R_j}{1 - M_j}\right). \quad (3)$$

The number of nontrivial equations represented by (3) is equal to i (corresponding to $V_i = 2, 3, \cdots, i + 1$), while there are $2 \cdot i$ unknowns (B_j and $C_j, j = 1, 2, \cdots, i$). An obvious closure condition that can be applied is to assume the amount of randomly overlapping clouds is proportional to the amount of minimally overlapping clouds (i.e., $R_j = a^*M_j$), so

$$V_{i+1} = [1 - (\sum_{j=1}^{i} M_j)] \prod_{j=1}^{i}\left(1 - \frac{a^*M_j}{1 - M_j}\right). \quad (4)$$

Separating the terms containing M_i gives

$$V_{i+1} = [1 - (\sum_{j=1}^{i-1} M_j) - M_i] \times \left(1 - \frac{a^*M_i}{1 - M_i}\right) \prod_{j=1}^{i-1}\left(1 - \frac{a^*M_j}{1 - M_j}\right). \quad (5)$$

Defining:

$$B_i \equiv 1 - \sum_{j=1}^{i-1} M_j, \quad (6)$$

$$C_i \equiv \prod_{j=1}^{i-1}\left(1 - \frac{a^*M_j}{1 - M_j}\right), \quad (7)$$

and substituting into (5) gives

$$V_{i+1} = [B_i - M_i]\left(1 - \frac{a^*M_i}{1 - M_i}\right)C_i. \quad (8)$$

Multiplying by $1 - M_i$ and collecting the M_i terms gives

$$(1 + a)\cdot M_i^2 + \left[-(1 + a)\cdot B_i - 1 + \frac{V_{i+1}}{C_i}\right]\cdot M_i + \left(B_i - \frac{V_{i+1}}{C_i}\right) = 0, \quad (9)$$

which is a quadratic in M_i. Equation (9) can be further simplified by recognizing that $V_i = B_iC_i$, and defining $F_{i+1} = V_{i+1}/V_i$:

$$(1 + a)\cdot M_i^2 + [-(1 + a - F_{i+1})\cdot B_i - 1]\cdot M_i + B_i\cdot(1 - F_{i+1}) = 0. \quad (10)$$

This equation can be solved using the quadratic formula, giving

$$M_i = \frac{-[-(1 + a - F_{i+1})\cdot B_i - 1] \pm \sqrt{[-(1 + a - F_{i+1})\cdot B_i - 1]^2 - 4(1 + a)B_i\cdot(1 - F_{i+1})}}{2(1 + a)} \quad (11)$$

which can be further simplified to

$$M_i = \frac{[(1 + a - F_{i+1})\cdot B_i + 1] \pm \sqrt{[(1 + a - F_{i+1})\cdot B_i - 1]^2 + 4aB_iF_{i+1}}}{2(1 + a)}. \quad (12)$$

The choice of "+" or "−" in the relation is not difficult: addition produces the unphysical result of $M_i > 1$, while subtraction always produces a physically realistic result. Proof of this assertion is contained in appendix A of Ramsey (1993). The system of equations is in lower triangular form and can easily be solved by back-substitution. Thus, a cloud field is calculated that meets the random/minimum assumptions given above and it is consistent with the ISCCP observations.

The bulk of this work is based on the random/minimum parameter $a = 0.5$. There is no firm fundamental basis on which to make this estimate, though it is similar to Tian and Curry's (1989) conclusion that on a 240-km scale the mean of the results from the minimum and random assumption produces the best results. Since the procedure inherently produces a cloud field consistent with top-of-atmosphere observations, OLR is not dependent on the parameter. Net Surface Longwave Radiation (NSLR) is dependent on the value, since a higher value results in more low cloud. The rationale for selection of $a = 0.5$ and the sensitivity of NSLR and the longwave profiles to the parameter is presented in section 5.

e. Adjustments for cirrus

As mentioned in section 2b, a significant problem with the ISCCP C1 IR-only data is misidentification of the high thin cloud. It is a necessary assumption of the IR-only analysis that the cloud be optically thick at the IR window channel wavelength. When this is not the case, the IR radiation from below the cloud will be transmitted through the cloud, resulting in an observed radiance that is higher than the blackbody radiance of a cloud at that level. Since the ISCCP cloud retrieval method correlates the IR radiance to the cloud-top temperature, which is used to infer the cloud-top pressure, high, thin clouds are often misidentified as lower-altitude clouds. The IR-VIS process overcomes this difficulty by observing the visible optical depth and modifying the analysis if the cloud is shown by the visible observations to be optically thin. Adjustments can then be made to the cloud-top height.

Since it was desired to use the IR-only data to permit both day and night calculations, a method was developed to adjust for this deficiency in the data. It is illustrated in Fig. 2. The idea is to estimate the number of cirrus-containing pixels in a grid box using the ISCCP visible data and to adjust the IR-only data accordingly. Prior to the adjustment step, the entire IR-VIS dataset is read and missing data is filled in by linear interpolation between the nearest previous and subsequent time points that have IR-VIS data. The thin cloud that is detected or estimated is removed from the lowest layer and a fraction of it is placed in the upper layer after the cloud overlap estimation algorithm (see section 2d) has been applied. This fraction is the cirrus emittance ϵ_{Ci}.

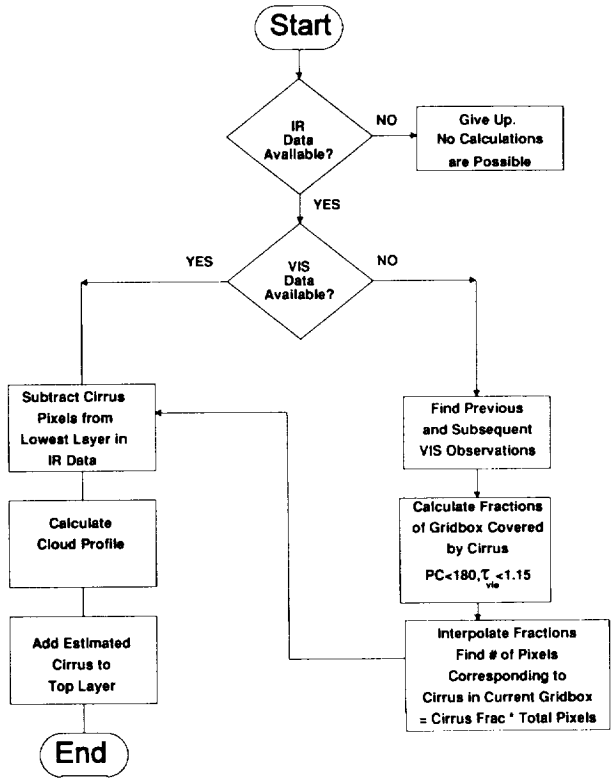

FIG. 2. Schematic diagram of cirrus adjustment technique.

f. Longwave parameterization

Longwave fluxes are calculated using the wide-band model described in Harshvardhan et al. (1987). This model is an emittance model and includes the effects of water vapor (two band centers, 0–340 cm^{-1} and 1380–1900 cm^{-1}, plus four band wings), carbon dioxide (620–720 cm^{-1} and wings), and ozone (980–1100 cm^{-1}). The model considers clouds to be black but permits fractional cloudiness, which is computationally identical to semitransparent clouds. The model was tested in the Inter Comparison of Radiation Codes for Climate Models (ICRCCM) (Ellingson et al. 1991) and it compared very favorably to the line-by-line calculations used as the baselines for that study. While this does not, in itself, guarantee that the model will produce accurate results, it is the best available indicator that the model is functioning properly with no obvious deficiencies relative to the baseline used in that study.

Briglieb (1992) compared a narrowband model, including extensive parameterizations of minor H_2O and CO_2 bands and trace gases, to the same model with only the major bands present. He found that the OLR over tropical oceans in the model lacking minor bands was 8–10 W m^{-2} higher than in the model with the more complete parameterization. It is thus expected that calculations with the Harshvardhan et al. (1987) model will show a similar bias when compared to observed clear-sky OLR.

The original model represented clouds as either maximally or randomly overlapped, consistent with the representation of convective and stratiform clouds in the Goddard Laboratory for Atmospheres general circulation model. For the reasons outlined in section 2d, the

cloud routines have been modified to use minimally and randomly overlapped clouds. Also, in the original model, presence of a maximally overlapped cloud superseded the presence of random cloud. To accommodate the cloud estimation routine used here, the model was revised so that randomly overlapped clouds do not occupy the area covered by minimally overlapped clouds. The fraction of each type of cloud is input independently, so that a layer can have any combination of randomly overlapping and minimally overlapping clouds.

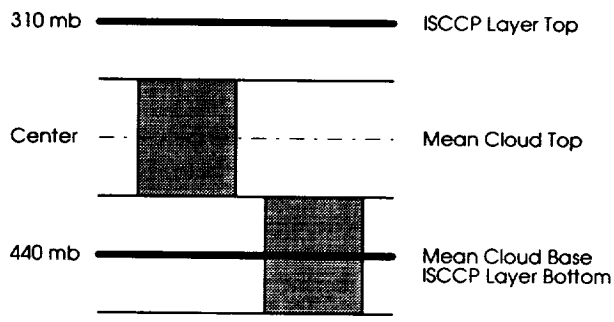

FIG. 3. Schematic showing placement of cloud in two sublayers.

g. Vertical discretization

The vertical discretization of the model was made to maintain the best correspondence to the seven-layer ISCCP C1 data while attempting to avoid creation of biases in final results. As such, the levels are based on the ISCCP cloud-layer bin limits, and the ECMWF data are vertically interpolated to match. According to Rossow et al. (1988) the mean values of the pressure can be assumed to be near the center of the category, at least for long-term means. While this study requires instantaneous values, it is still reasonable in the absence of other information to require that the mean cloud top be at the center of the ISCCP layer. The ISCCP layers are quite thick, 120–200 hPa, which is probably much thicker than real clouds. To place the clouds with the tops at the center of their layer, and the bottom at the center of the layer below, would excessively increase the downward longwave flux at the surface, which reduces NSLR. Placing the cloud in the lower half of the layer with the base at the bottom would introduce artificial oscillations into the flux divergence profile because the top half of a layer would always be cloud free.

It was decided to partition the layers and put half of the observed cloud in the top half and the other half in the lower part. The ISCCP defined layers are divided into two layers with tops at 25% and 75% of the pressure difference between the original layer limits, as shown in Fig. 3. Half of the detectable cloud is placed in each sublayer so that the total cloud coverage as viewed from space is unchanged and the mean cloud-top height is at the center of the original ISCCP layer. The mean base generated by this procedure is at the bottom of the original ISCCP layer. Because of the way the overlap scheme works (see section 2d), there is more cloud in the lower half of the revised layer than in the top whenever there is a random overlap component. This is required because the top layer partially obscures the lower layer, hence, more cloud is required to make the field consistent with the observations. Thus, the area-weighted-mean cloud base is actually slightly lower than the location indicated in Fig. 3.

For the near-surface cloud bases, a different approach is used. There are always two layers bounded by 850 hPa and the surface. If no cloud is detected in the lowest ISCCP layer (800–1000 hPa) the layers are separated at 931 hPa. If cloud is detected, it is contained in a layer that is bounded by 850 hPa and the mixing condensation level, and a clear layer extends from the MCL to the surface. The MCL is found from the upper-air data at 1000 and 850 hPa. Temperatures and specific humidities are used to establish the atmospheric condition, assuming that $\partial\theta/\partial p$ and $\partial q/\partial p$ were constant before mixing occurred in the subcloud layer. The MCL is found using an iterative approach. Iterations are performed until the process either converges or gives a value greater than 990 or less than 860 hPa. This guarantees that there is always a clear layer below the MCL and always a cloudy layer at least 10 hPa thick whenever clouds are detected by ISCCP.

There are two stratospheric layers, from 82.5 (the 75% point of the ISCCP 180–50-hPa layer) to 1 hPa. The radiation code also requires a 1–0-hPa layer. Stratospheric specific humidity is fixed at 2.5 10^{-6} g/g, and the temperature is interpolated from the ECMWF 50-hPa temperature to 270 K at 1 hPa. At all levels, temperature is interpolated in the logarithm of pressure from the original levels to the new levels, and the logarithm of the specific humidity is interpolated in the logarithm of pressure.

3. Clear-sky OLR

As a first test of the model, clear-sky OLR values were calculated at all grid points in the region bounded by 15°S–15°N, 150°E–120°W for several months and compared to the ERBE clear-sky values. A summary is shown in Fig. 4. It is clear that there is a serious discrepancy in January 1986, while May through July 1986 results compare more favorably even though there is a noticeable bias. The January discrepancy is most likely due to the addition of satellite water vapor information to the assimilation scheme on 11 March 1986. Because of these differences, no results prior to May 1986 will be subsequently used. The bias seen in the May through July results, which consists of OLR values being higher than those from ERBE, is attributed to a combination of the model deficiencies mentioned in section 2f, as well as to insufficient upper-tropo-

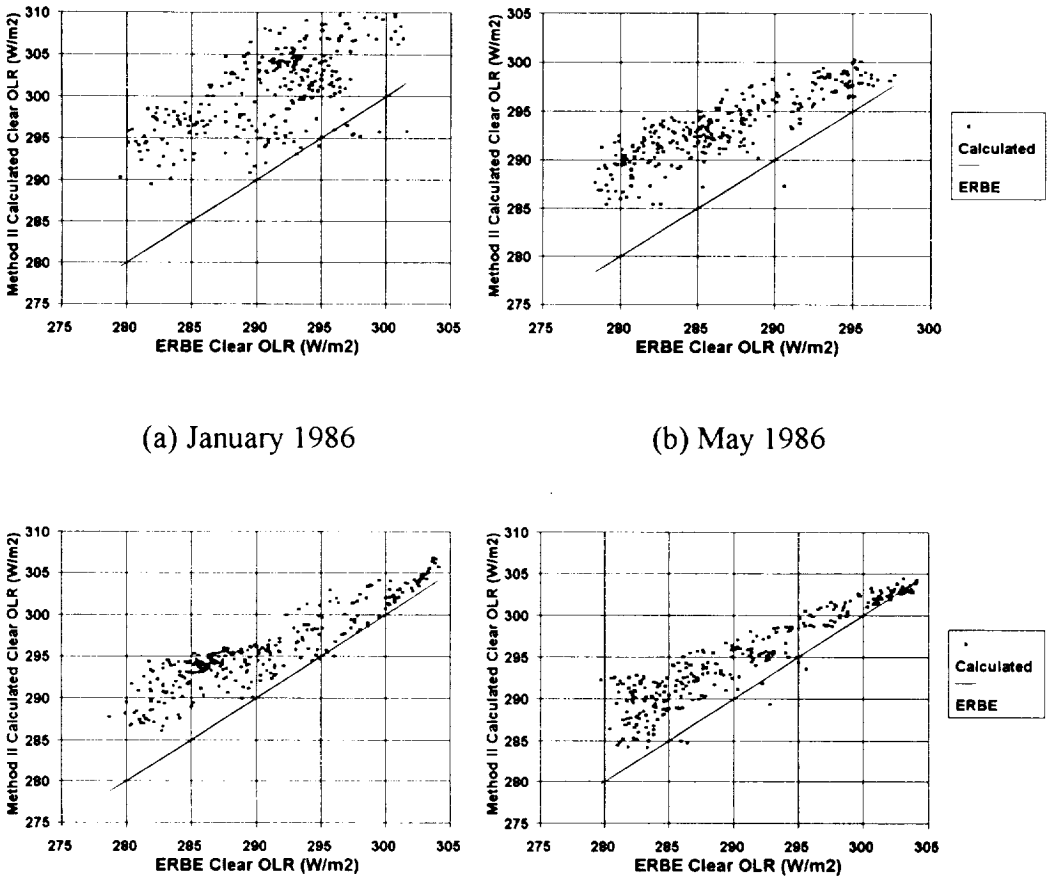

FIG. 4. Calculated and ERBE clear-sky OLR in W m $^{-2}$ for January, May, June, and July 1986.

spheric water vapor in the ECMWF analyses (Trenberth 1992).

4. All-sky OLR

a. Cirrus emittance

OLR is strongly affected by high clouds, so the cirrus emittance parameter ϵ_{Ci} was calibrated by comparing OLR values calculated using several ϵ_{Ci} to results from ERBE. Cirrus emittance values of 0.10, 0.20, 0.40, 0.50, and 0.66 were used to calculate cloud amount profiles and those profiles used to calculate outgoing longwave radiation fields for the month of July 1986. An OLR calculation using an unadjusted cloud profile was also made. Scatter diagrams for the same region as in Fig. 4 are shown in Fig. 5 and depict the relationship between ERBE and calculated OLR for the unadjusted profile and for ϵ_{Ci} = 0.10, 0.30, and 0.66. For the unadjusted profile, there is considerable discrepancy at the low end of the scale, with absolute errors approaching 20 W m^{-2}. Use of ϵ_{Ci} = 0.66 is an obvious overcorrection, with low biases and increased scatter throughout the range. For ϵ_{Ci} = 0.30, it appears that there remains the problem of excessively high OLR at the low end of the scale, but the random error is reduced.

The absolute bias is considered not to be the best parameter on which to base the optimization. This is because the clear-sky results calculated above indicate a general high bias in the method so that the emittance, which reduces the bias to zero, is probably overcompensating by introducing excessive amounts of high cloud. For this reason, differences, rms errors, and correlation coefficients were calculated and are shown in Fig. 6. It is seen that the rms error is minimized at ϵ_{Ci} = 0.40, but the correlation is highest at ϵ_{Ci} = 0.20. A compromise between these two considerations of optimization was made, and ϵ_{Ci} = 0.30 was chosen for all subsequent work.

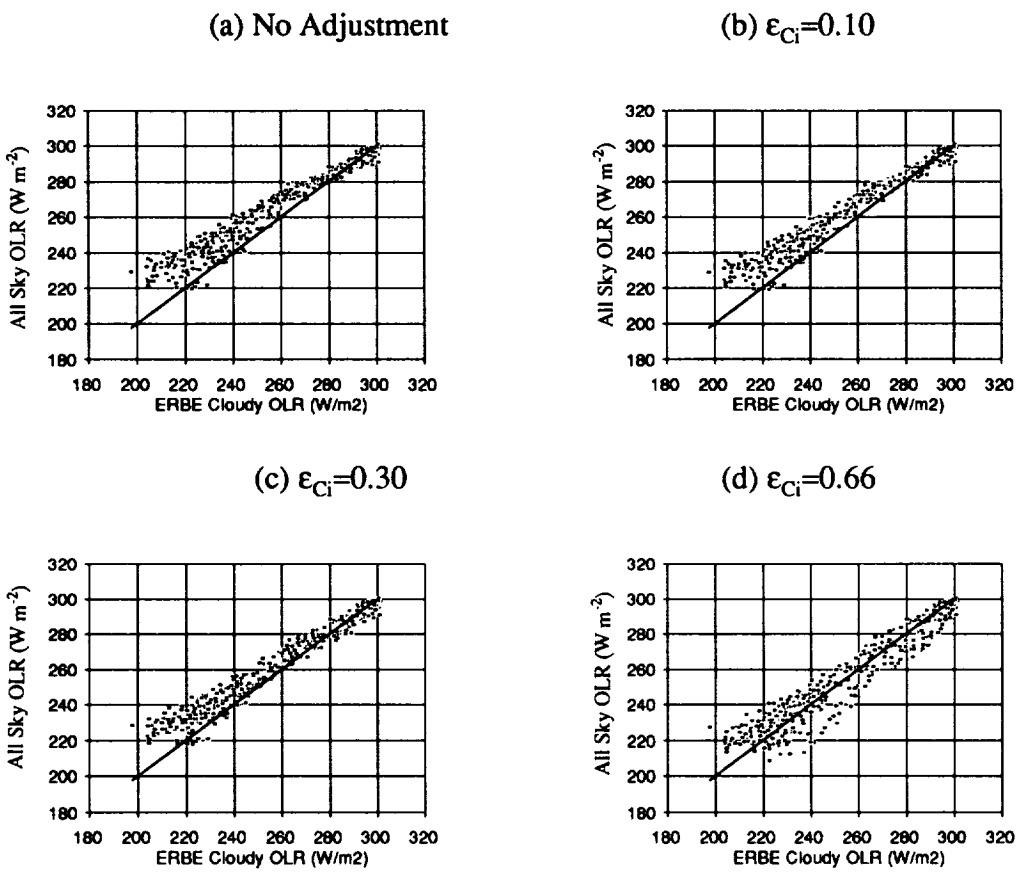

FIG. 5. Relationship between calculated and ERBE cloudy-sky OLR for several values of the cirrus emittance parameter ϵ_{Ci}. Values are in W m^{-2}.

b. OLR fields

Using the cirrus emittance ϵ_{Ci} = 0.30, cloud fields were calculated and used to calculate all-sky OLR. Maps of calculated and ERBE OLR for May, June, and July 1986 are shown in Figs. 7, 8, and 9, respectively. The top panel of each map is the calculated OLR, the middle panel is ERBE OLR, and the bottom panel is the difference field. Note that the contour interval of the OLR maps is 10 W m^{-2} but for the difference field it is 5 W m^{-2}. In general, the pattern agreement between the two fields is quite good, particularly with respect to the placement of secondary features such as the relative minimum near the date line in the ITCZ for July. The gradient from east to west, however, is lower in the calculated field than ERBE. Specifically, in the western edge of the domain the calculated values are typically 15 W m^{-2} higher than ERBE. This is a repetition of the type of discrepancies noted in the clear-sky and cirrus emittance tests, though it is of larger magnitude.

Scatter diagrams for all grid points within the region shown are given in Fig. 10 for each of the 3 months. These figures confirm the observations made with the maps. The regression coefficients for the 3 months are shown in Table 1. The r^2 values are typically 0.96, and a typical regression function is $OLR_{ERBE} = 50 + 0.8 * OLR_{CALC}$. This indicates that the modeled OLR is following the trends in the overall observed field, though the gradients from west to east are too low. The difference in the mean could be attributed to difficulties with the radiation parameterization, but the errors in the gradient would be of the opposite sense if this were the only problem. It is more likely that the ECMWF water vapor gradients are too weak. The errors in the all-sky analyses are approximately the same as in the clear-sky analyses, lending credence to this conclusion.

c. Sensitivity to tropospheric water vapor

Because of the uncertainty in the quality of analyzed fields of upper-tropospheric water vapor, some sensitivity studies were made. One analysis involved multiplying the upper-tropospheric (above 470 hPa) specific humidity by a fixed amount over the entire region and comparing OLR and heating profiles. OLR was calculated from the baseline humidity and from 125%, 150%, and 200% of the baseline values. Examination

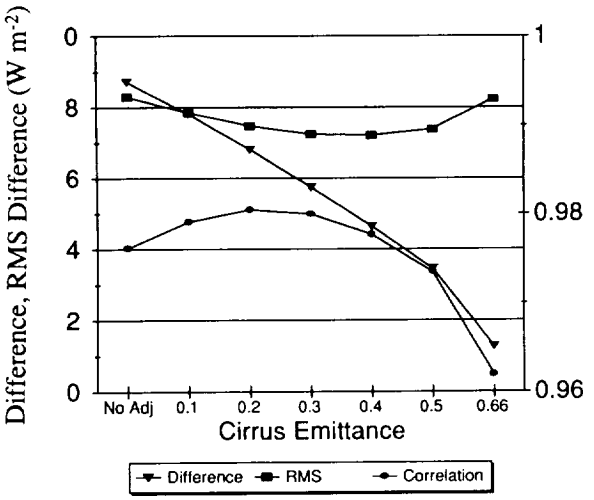

FIG. 6. Differences in W m $^{-2}$ and correlation between calculated and ERBE cloudy-sky OLR for several values of the cirrus emittance parameter ϵ_{Ci}.

of the differences between the calculated fields (not shown) indicated that the effects of the changes were quite uniform spatially, with OLR approximately 2 W m^{-2} lower than the baseline value for the 150% case and 3.5 W m^{-2} lower for the 200% case. Figure 11 shows the mean differences, rms differences, and correlation coefficients between the four calculated OLR fields and ERBE. The correlation increases as upper-tropospheric humidity increases, but a close examination reveals that the increase is very slight. The impact of these changes on the distribution of longwave cooling will be examined in section 6c.

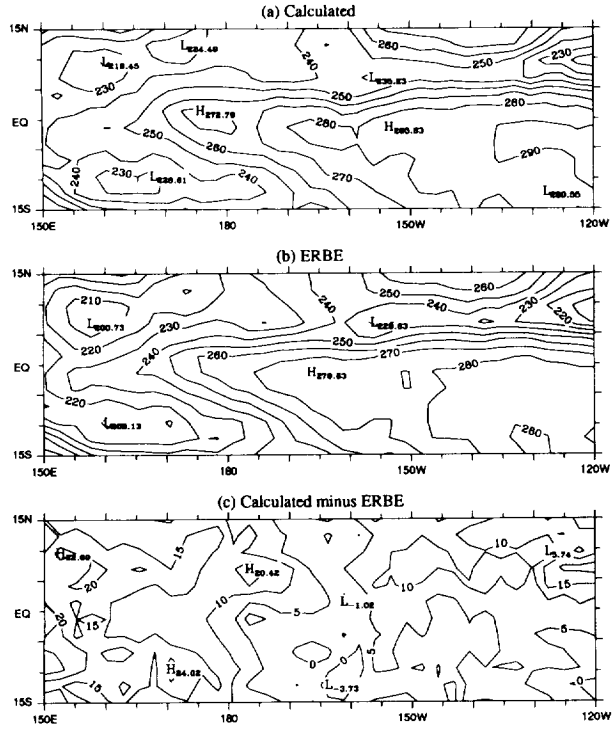

FIG. 7. Calculated and ERBE cloudy-sky OLR in W m $^{-2}$ for May 1986.

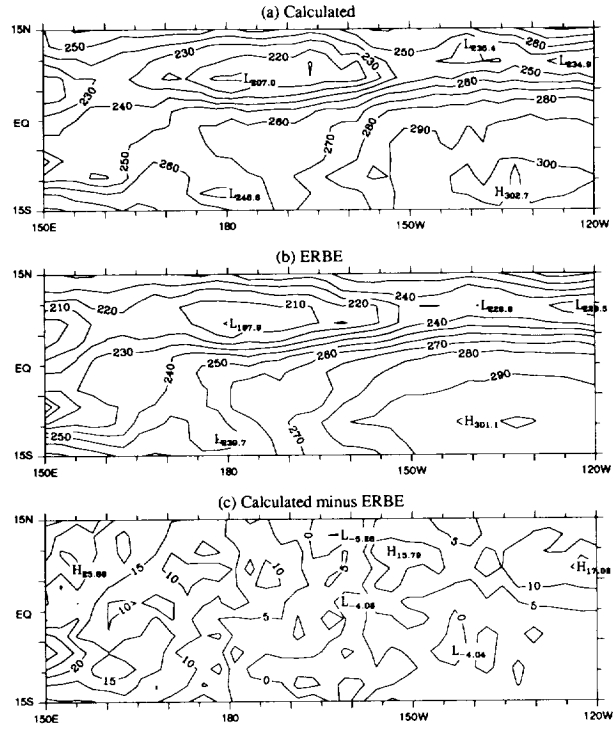

FIG. 8. As in Fig. 7, except for June 1986.

5. NSLR and sensitivity to cloud overlap parameter

To test the sensitivity of the method to the assumed cloud overlap parameter (see section 2d), cloud fraction profiles were calculated based on several different overlap parameters and compared to data from a cloud atlas. Maps of NSLR were calculated from these profiles. Since no reliable large-scale observations of NSLR exist, results can only be compared to each other to determine their sensitivity to the cloud overlap parameter.

Cloud profiles were calculated for January and July 1986 for cloud overlap parameters of 0 (all minimum overlap), 0.5, 1, and 2. January and July 1986 were chosen to represent different times of the year while avoiding the El Niño that began influencing the region in the latter half of 1986 (Climate Analysis Center 1986a,b). The region of interest was then subdivided into nine regions, as shown in Fig. 12. To test these calculated cloud amounts, the ocean cloud atlas of Warren et al. (1988) was used. This atlas is a summary of cloud cover reported in the 1952–81 Comprehensive Ocean–Atmosphere Data Set. Clouds of type "cumu-

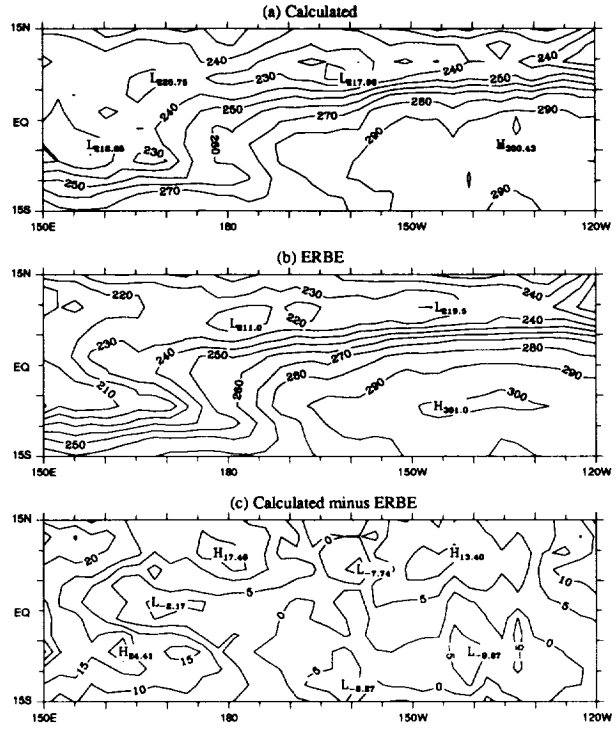

FIG. 9. As in Fig. 7, except for July 1986.

lus'' and stratus-type clouds (''stratus + stratocumulus + fog'') are considered to be most representative of clouds seen by the observer on the ground. Type ''cumulonimbus'' is not included in this analysis because it only covers a small fraction of the ground (Riehl 1979). It is assumed that the best estimate of ground cover is to add the atlas cloud amounts and that this sum corresponds to the calculated mean cloud amounts in the lowest three cloud layers. That comparison is made in Figs. 13 and 14. The bars on the figures represent the atlas data, and the numbers in each column show the low cloud fraction calculated for each overlap parameter. While the agreement between these two independent estimates is not expected to be exact, they provide at least some evidence that the combined random/minimum estimation method gives better results than either the minimum or random assumption alone. An overlap parameter of 0.5 provides the best agreement with the atlas data and was used for the main body of this work.

Maps of net surface longwave radiation were generated for overlap parameters of 0, 0.5, and 2.0, and are shown in Fig. 15. The patterns of NSLR are quite similar for all of the values analyzed. Virtually no differences are seen in the less cloudy regions, with some differences in the cloudy regions. A scatter diagram showing the individual averages compared to the $a = 0.5$ case is shown in Fig. 16. This confirms the conclusion that in clear regions the overlap parameter is not of great importance, while in the cloudy areas it can make a difference in the monthly mean of up to 5 W m^{-2}. Based on the results of this section, it seems unlikely that the overlap parameter can exceed 1, making the uncertainty in the final NSLR less than 2.5 W m^{-2}, even in the most extreme cases.

6. Vertical profiles of longwave radiative cooling

The vertical profiles of longwave cooling were calculated for the months of June 1986 through June 1987. November 1986 was not used due to missing ISCCP data. Selected results are examined here in detail and are compared to results from prior studies. In addition to the baseline results, effects of modification of the upper-tropospheric water vapor, cloud amount, and cloud overlap parameter are examined.

a. Comparison to previous results

Figure 17 shows the monthly mean longwave profile in regions NW and SE (as defined in Fig. 12) for the month of July 1986, along with the associated monthly mean cloud amounts in each time period. The key difference between the two is the considerable longwave cooling near the surface in the SE profile. This is attributed to lower water vapor content, as well as less cloud, providing a clearer path from the lower troposphere to space. These results are compared with the results of Dopplick (1970), Cox and Griffith (1979) (hereafter CG), and Ackerman and Cox (1987) (hereafter AC) in Fig. 18. The profile for the current work is the July 1986 profile averaged over the entire analysis domain. The Dopplick profile is a climatological average for June, July, and August at 10°N. The CG profile is for Phase III of GATE and was compiled for A/B-scale ship array. The AC profile is from their Fig. 17 and is an average over the four phases of the summer monsoon in the eastern Arabian Sea. Ackerman and Cox presented total radiative heating, so the CG shortwave profile was subtracted from total radiative heating to produce an estimate of their longwave profile. The shapes of the four profiles are quite similar, with very good agreement between Dopplick's and the one from the present method. The other two profiles differ somewhat, with this work indicating less cooling at the surface and at the tropopause and more cooling at the midlevels. Of particular interest is the location of the maximum cooling: in this work, it is higher than in either CG or AC, and the magnitude is greater than that given by Dopplick. It is difficult to assess the reasons for the detailed differences between these profiles, since they use different data assumptions and radiation parameterizations and they are for different domains and periods.

b. Sensitivity to cloud overlap parameter

The effect of the cloud overlap parameter on the vertical profile of longwave cooling was examined by cal-

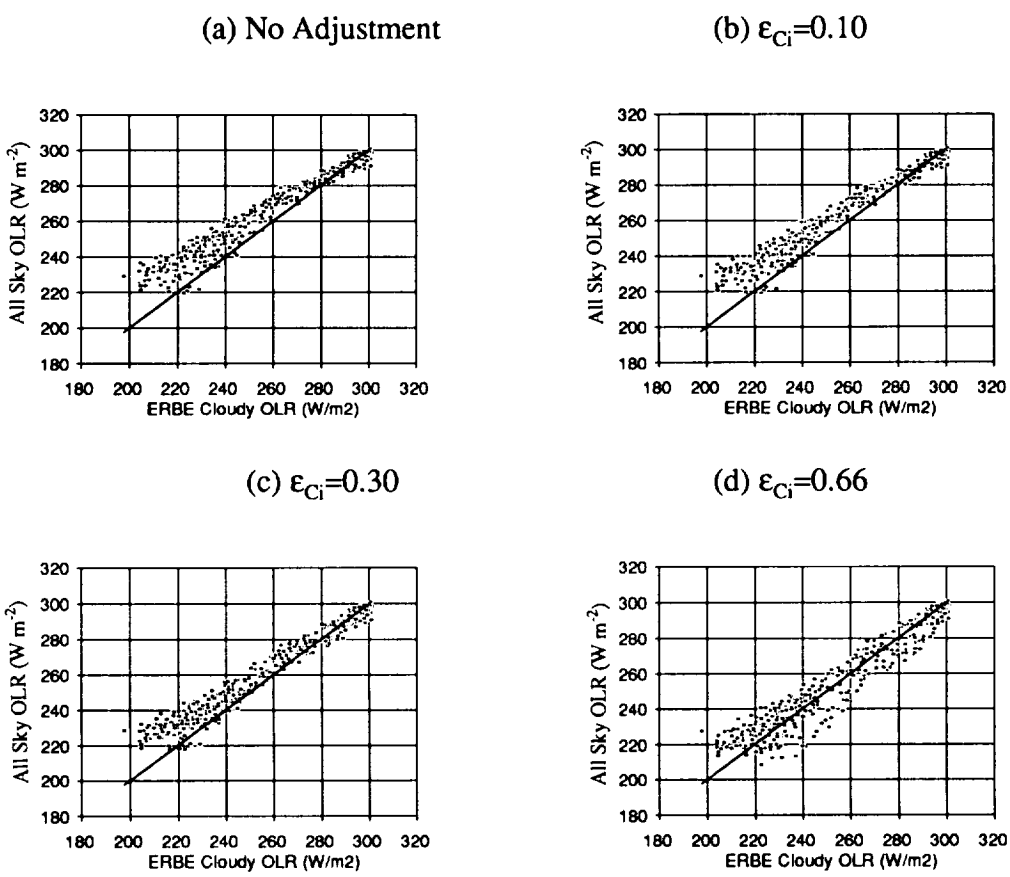

FIG. 10. Scatter diagrams showing relationship between calculated and ERBE cloudy-sky OLR. Values in W m^{-2}.

culating profiles using extreme values of 0 (minimum overlap) and 2 for the overlap parameter. Figure 19 shows the longwave cooling profile for the NW region using these parameters, along with the baseline value of 0.5. The profiles are quite similar, except that near the surface there is slightly stronger near-surface cooling (~0.4°C day^{-1}) and slightly weaker midtropospheric cooling (~0.4°C day^{-1}) for the a = 0 case relative to the a = 2 case. This is as expected because less low cloud means that there can be greater net flux at the surface but weaker emission at the midlevels. Figure 20 shows the results for the SE region; only the a = 0 profiles is shown because the other two are virtually coincident. As expected, the cloud overlap parameter is of no consequence in this area, which is virtually free of high- and midlevel clouds.

TABLE 1. Regression results for calculated and ERBE cloudy-sky OLR for May, June, and July 1986.

	May	June	July
Constant	58.2	50.8	47.0
R Squared	0.96	0.95	0.97
X Coefficient(s)	0.792	0.816	0.825
Std Error of Coeff	0.008	0.009	0.007

c. *Sensitivity to upper-tropospheric water vapor*

Figure 21 shows the longwave profiles for the NW region (as defined in Fig. 12) for the baseline and 200% humidity cases analyzed in section 4c. Above 470 hPa, there is a slight increase in the cooling rate for the 200% water vapor case. The differences among extreme profiles in the upper troposphere are always less than 0.5°C day^{-1}, indicating that reasonable errors in the analysis of upper-tropospheric water vapor probably do not have an overwhelmingly large impact on the final results. At 500 hPa, there is a sharp decrease in the cooling rate, but this is due to the rapid change in the water vapor field used in this sensitivity study. The high downward longwave flux that is a consequence of the doubled water vapor reduces the cooling below. Thus, this should not be considered a relevant feature.

A substantial change in the ECMWF model on 2 May 1989 significantly altered the upper-tropospheric water vapor characteristics. A second humidity sensitivity study compared the impact of this change on the longwave flux profiles. Figure 22 summarizes the dif-

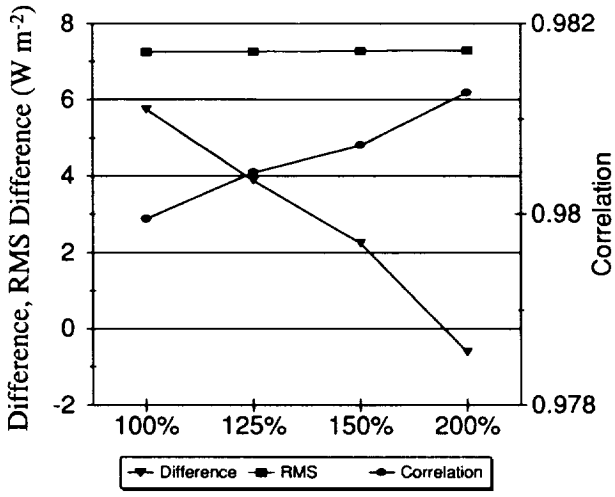

FIG. 11. Difference between ERBE OLR and OLR calculated using increased upper-tropospheric water vapor, July 1986. Also shown are rms differences and correlation coefficients. All values in W m^{-2}.

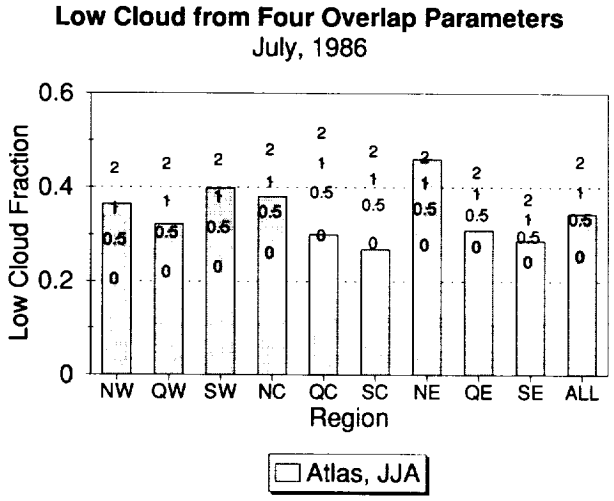

FIG. 13. Cloud fraction in lowest layers for January 1986 compared to Warren et al. (1988) atlas for December, January, and February.

ferences in clear-sky profiles before (July 86 and April 89) and after (May and July 89) the incorporation of the mass flux scheme on 2 May 1989. Clear-sky profiles are shown because of a substantial reduction in the availability of ISCCP data in the eastern portion of the region early in 1989 due to the loss of *GOES-6* (Rossow and Schiffer 1991). The profiles are quite similar in appearance, though there is some tendency for the 300–400-hPa cooling to be less after 2 May 1989. In any case, the difference does not exceed the month-to-month natural variability. It is concluded from these results that, although there appears to be some impact due to the changes in the assimilation scheme, they are not large enough to invalidate the basic radiation results.

d. Spatial and temporal variability

An important goal of this study is to quantify the spatial and temporal variability of radiative cooling. First, the usefulness of approximating the monthly mean at each point in space by the grand mean over the entire domain was examined. The monthly mean cooling rate at each point was found, and the standard deviations in space of the monthly means over the entire domain were calculated for July 1986. Mean ($\bar{x}$) and mean plus or minus two sample standard deviations ($\bar{x} \pm 2s$) are shown in Fig. 23. A similar result for December 1986 is shown in Fig. 24. The $\bar{x} \pm 2s$ limits may be interpreted as the range into which 95% of the point-wise monthly means would be expected to fall. The upper-tropospheric variation is approximately 0.5°C day^{-1} over this timescale but below 700 hPa the variation is about 1°C day^{-1} in a quantity with a magnitude of 2°C day^{-1}. From this, we conclude that to

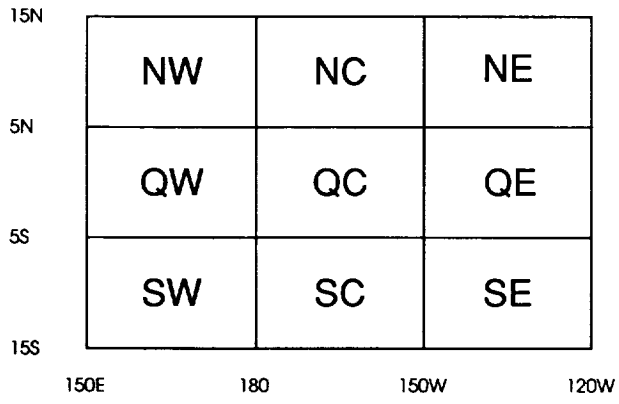

FIG. 12. Map of regions analyzed.

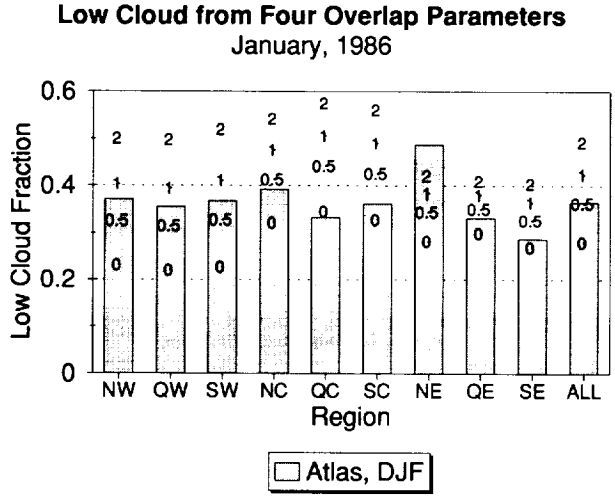

FIG. 14. As in Fig. 13, except for June, July, and August.

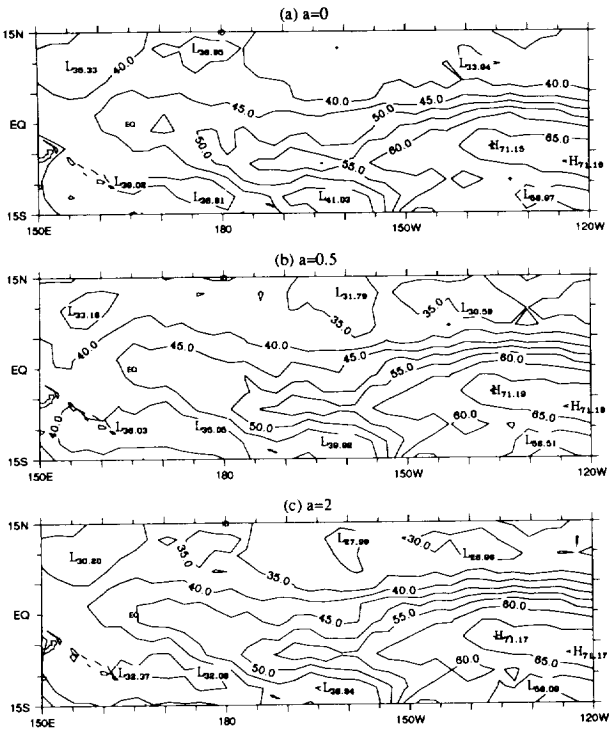

FIG. 15. Net surface longwave radiation in W m^{-2} for overlap parameter a = 0, 0.5, and 2, July 1986.

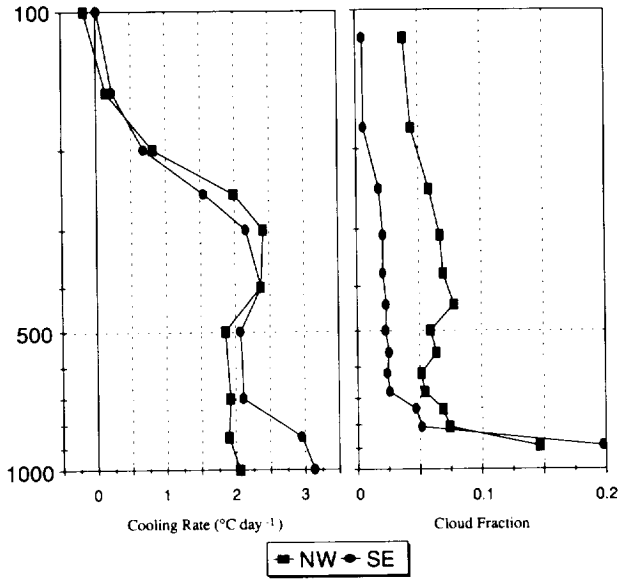

FIG. 17. Longwave cooling profiles in °C day^{-1} for two regions. The NW is predominantly cloudy, the SE clear.

assume that the monthly mean of the entire domain can be represented by a single profile is probably not acceptable.

Second, the usefulness of approximating the instantaneous magnitude of the cooling at a point by the long-term mean was examined. Time series of the twice-daily longwave cooling were constructed, and the temporal mean and standard deviation at each point in space were found. The time series for an arbitrarily selected point within NW region (8.75°N, 171.25°E at 700 hPa) is

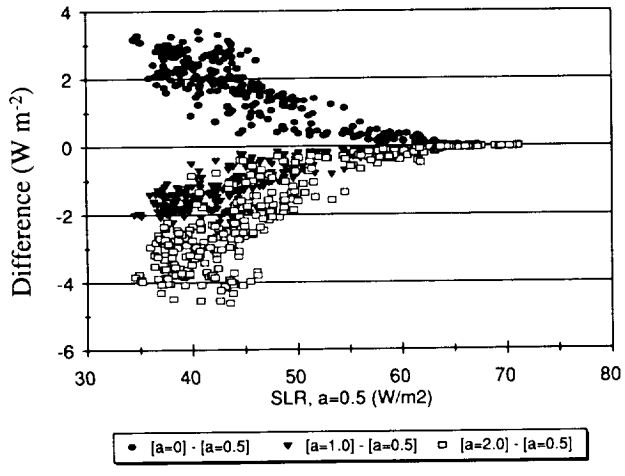

FIG. 16. Differences between NSLR fields in W m^{-2} calculated by subtracting overlap parameter a = 0.5 from a = 0, a = 1, and a = 2 for July 1986.

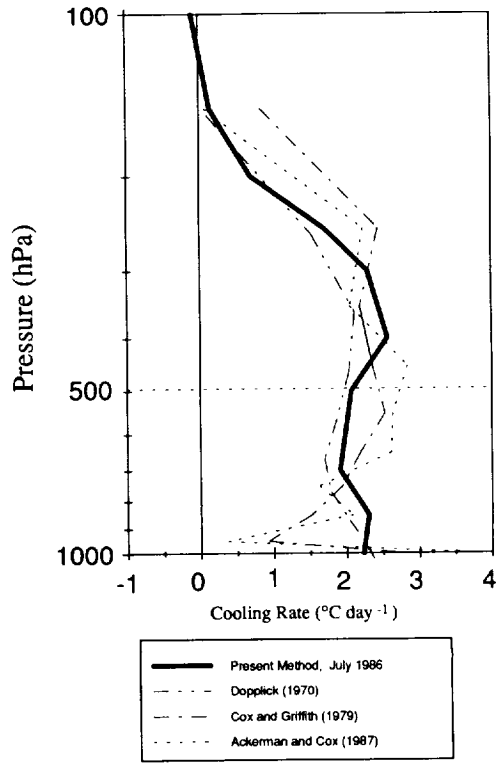

FIG. 18. Comparison of longwave profile in °C day^{-1} to previously published studies. Values °C day^{-1}.

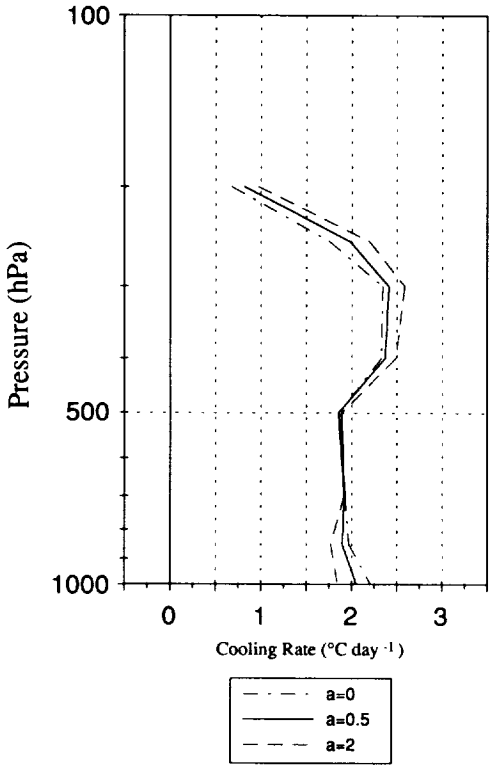

FIG. 19. Comparison of the effects of the cloud overlap parameter in the longwave cooling profile for NW region, July 1986. Values °C day^{-1}.

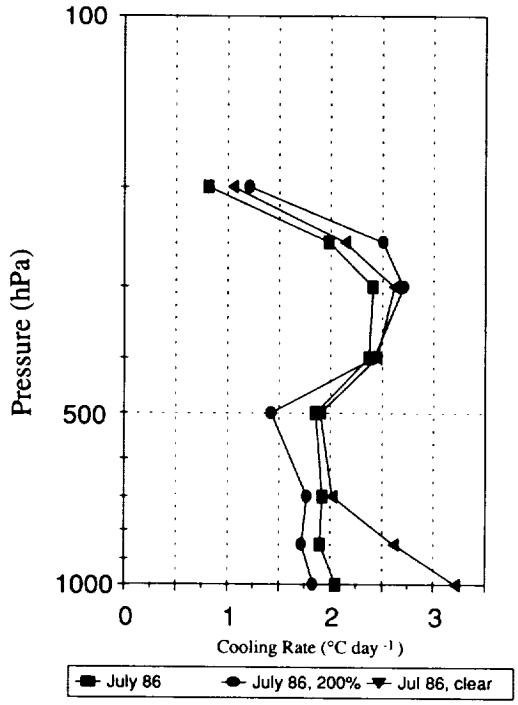

FIG. 21. Comparisons among longwave cooling profiles in °C day^{-1} for original values, increased upper-tropospheric water vapor, and a clear sky using baseline water vapor; all for July 1986.

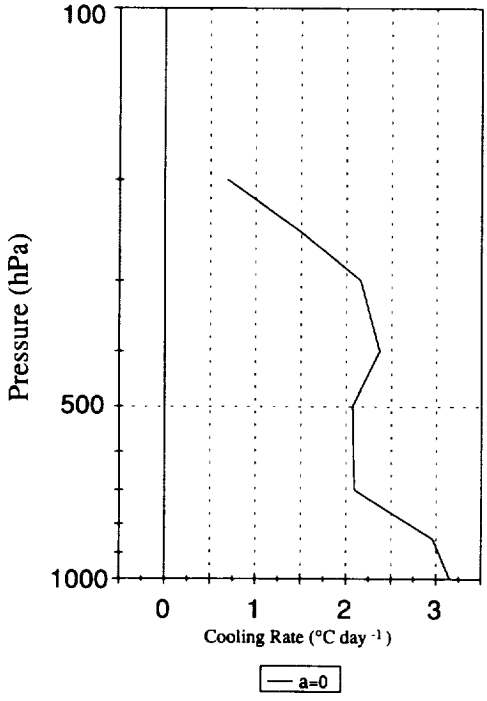

FIG. 20. As in Fig. 19, except for SE region, July 1986, and only for $a = 0$ overlap parameter.

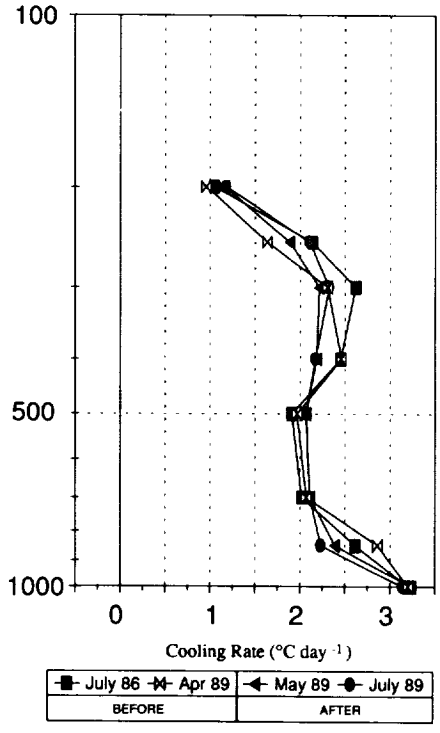

FIG. 22. Clear-sky longwave radiative cooling profiles in °C day^{-1} before and after incorporation of revised convective parameterization on 2 May 1989.

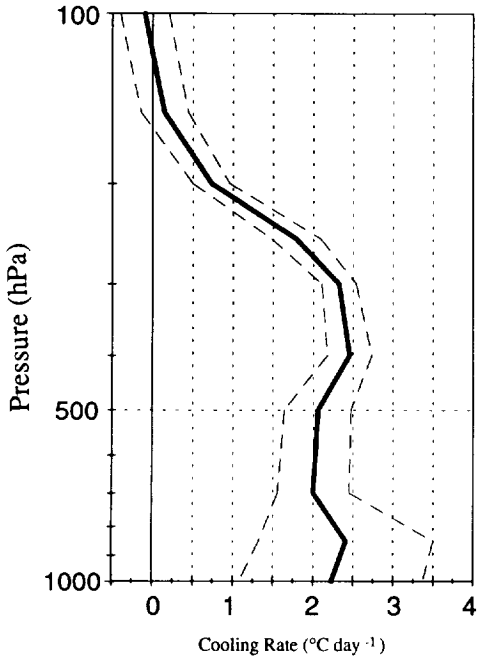

FIG. 23. Mean and plus or minus two times standard deviation of longwave cooling over the entire analysis domain, July 1986. Values in °C day $^{-1}$.

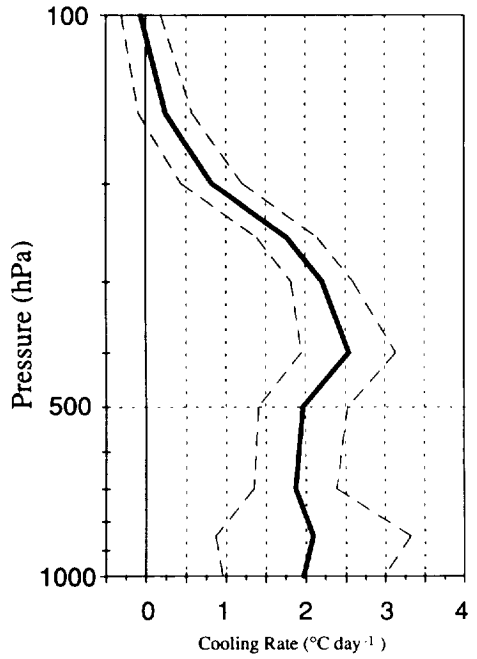

FIG. 24. As in Fig. 23, except for December 1986.

shown in Fig. 25. The area outside the $\bar{x} \pm 2s$ limits is shaded, where $\bar{x}$ and s are the individual mean and standard deviation calculated for this particular time series. It would be expected that about 5% of the approximately 600 sampled values would be outside the $\bar{x} \pm 2s$ limits, and indeed, 6% are. Histograms of the data were created using 0.1°C day^{-1} bins. The expected amounts, assuming that the data are distributed normally, are shown along with the histogram in Fig. 26 for the NW region and Fig. 27 for the SE region. The distribution is not far from normal, although there is a second mode near 1°C day^{-1} in both cases. Thus, the distributions are represented to a good degree of accuracy by a normal distribution, but care must be used in the interpretation of confidence limits generated due to the nonnormality of the distribution. Limits on a multiperiod mean could be estimated by taking the standard deviation of the mean, which is equal to $(sN^{-0.5})$, where N is the number of values sampled. The 95% limit on a five-day mean, therefore, is $10^{-0.5}$ or about one-third as wide as the single-period limits. This argument strictly holds only if the mean being approximated is based on uncorrelated random samples, a requirement that may not be valid for ten sequential observations. In practice, therefore, the error limits are larger.

To develop a regional picture of the temporal variability, these means and standard deviations in time were averaged over each of the nine regions. Figures 28 and 29 show the mean and $\bar{x} \pm 2s$ limits for the regions NW and SE, respectively. The 95% confidence limits are seen to be approximately ±1°C day^{-1} throughout most of the troposphere, with considerably larger limits near the surface in the SE region. Similar results were generated from clear-sky profiles to determine the effects of clouds. These results are shown in Figs. 30 and 31 and correspond to Figs. 28 and 29, respectively. The 95% confidence limits are seen to be about one-half as wide as in the all-sky case, indicating that approximately one-half of the temporal variability can be attributed to clouds.

7. Summary and conclusions

Longwave cooling over the Pacific ocean was calculated from June 1986 through June 1987. To accomplish this, longwave radiation was calculated using the ECMWF/WCRP TOGA Archive II dataset and ISCCP C1 IR-only cloud data in a broadband longwave flux model. Clear-sky OLR was calculated and was found to agree, in general character, with ERBE clear-sky observations; however, the calculated fluxes were too high in the moist part (western sector) of the region. This discrepancy was probably due, in part, to insufficient water vapor in the analyses, as well as to errors in its distribution. Because of misidentification of thin clouds by the ISCCP IR-only algorithm, an adjustment mechanism was developed. Results for selected months were used to calibrate the cirrus adjustment procedure. Based on the adjusted cloud profile, cloudy-sky OLR was calculated and compared to ERBE results. Cloudy-sky results showed approximately the same bias relative to ERBE as the clear-sky results: low values too high and high values too low.

A method was developed to estimate low cloud from the ISCCP observations based on the assumption that

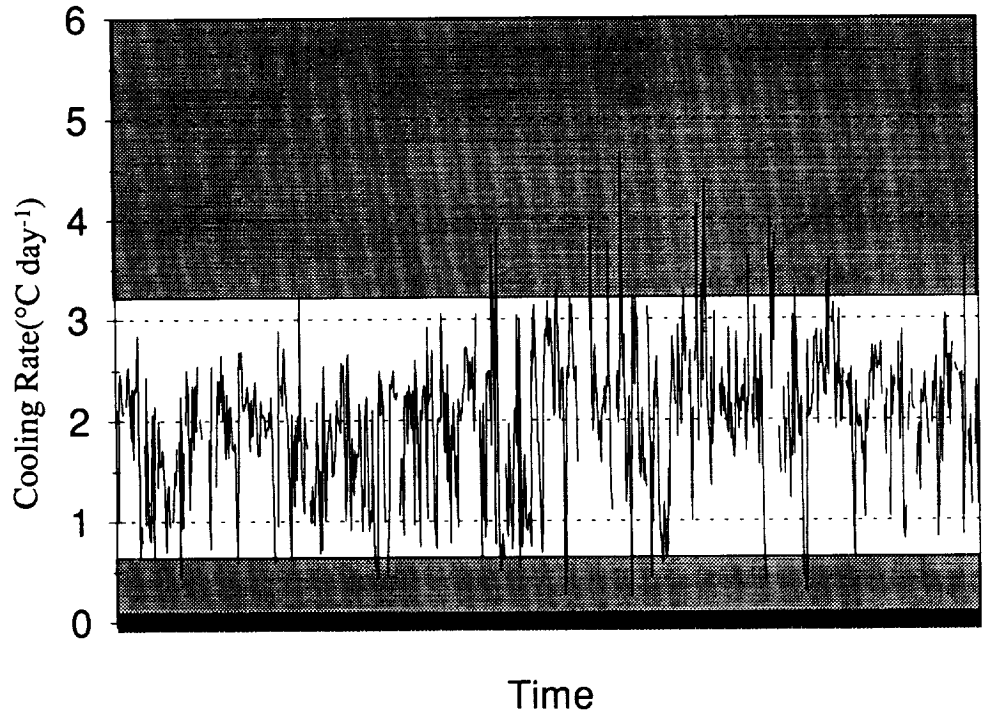

FIG. 25. Time series of longwave cooling rates in °C day $^{-1}$ at 8.75°N, 171.25°E, 700 hPa. The shaded areas are outside the $\bar{x} \pm 2s$ limits.

clouds can be represented as a combination of randomly and minimally overlapped clouds, with a parameter that can be used to tune the low cloud amount. Monthly mean values of NSLR were calculated and found to vary from approximately 75 W m^{-2} in the east Pacific to 35 W m^{-2} in the west. NSLR was only minimally affected by the parameter of the overlap scheme; over a range of reasonable values, NSLR was affected by not more than ±2.5 W m^{-2}.

Vertical profiles of longwave cooling were found to be similar to results from previous studies, with the maximum in longwave cooling slightly higher in the troposphere than was found in other work. Over the range of possible overlap values, the monthly mean cooling rate did not change by more than 0.2°C day^{-1}.

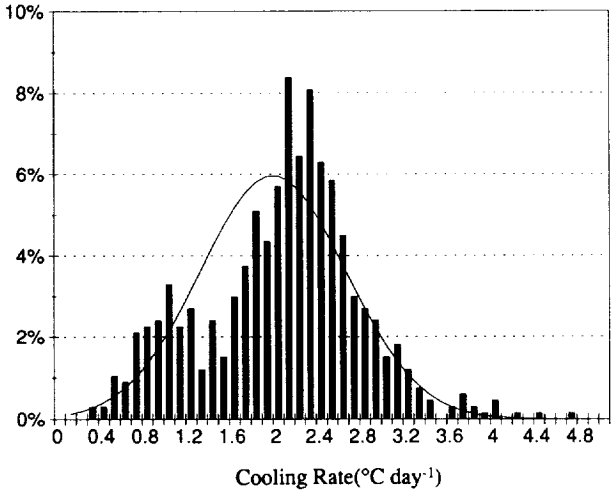

FIG. 26. Histogram of longwave cooling rates in °C day^{-1} at 8.75°N, 171.25°E, 700 hPa. Solid line represents $N(\bar{x}, s^2)$.

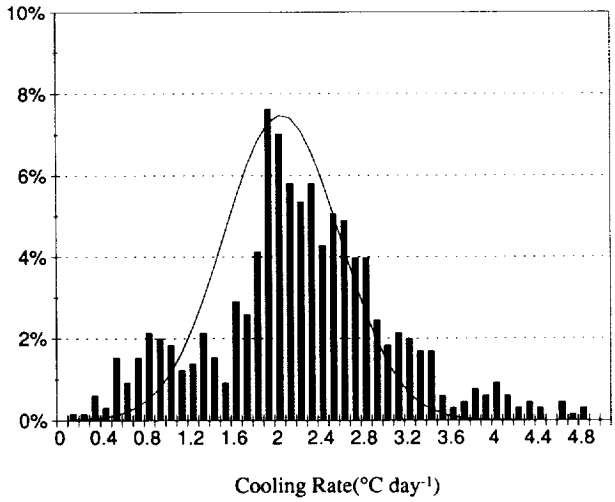

FIG. 27. As in Fig. 26, except for 8.75°S, 138.25°W.

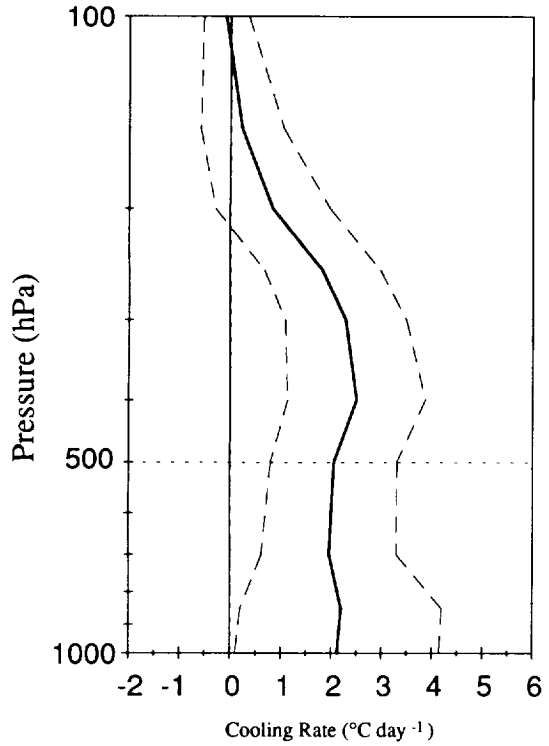

FIG. 28. $\bar{x} \pm 2s$ of longwave cooling in °C day $^{-1}$ for NW region.

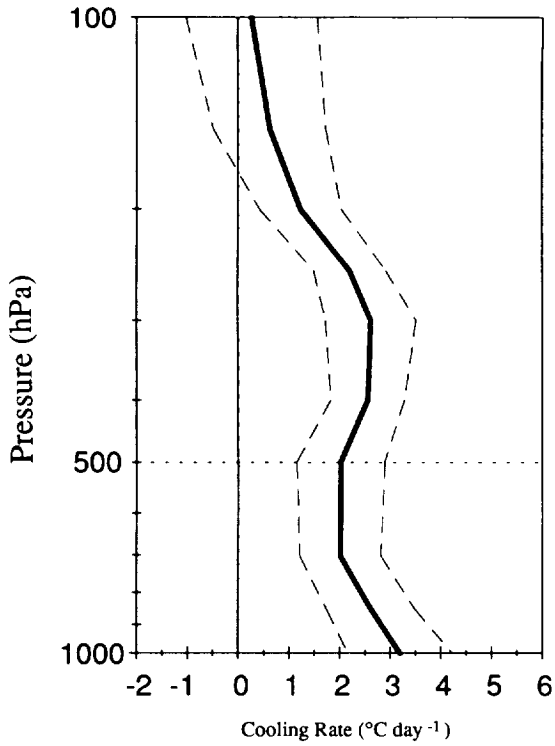

FIG. 30. The $\bar{x} \pm 2s$ of clear-sky longwave cooling in °C day $^{-1}$ for NW region.

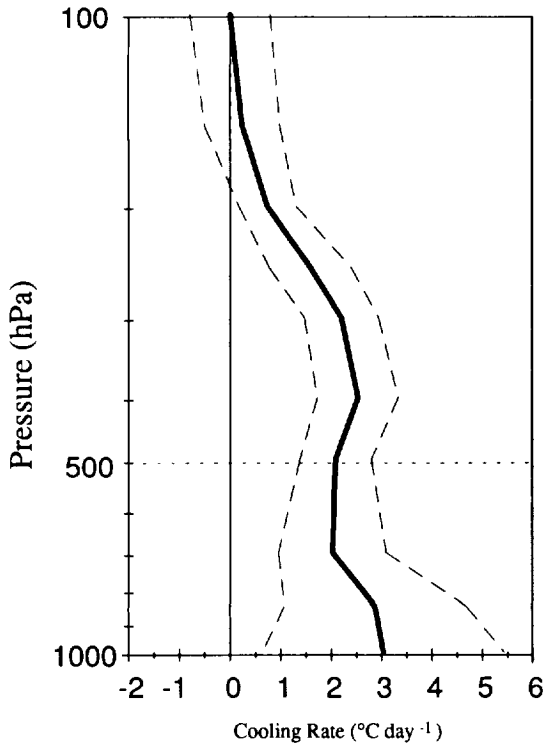

FIG. 29. As in Fig. 28 except for SE region.

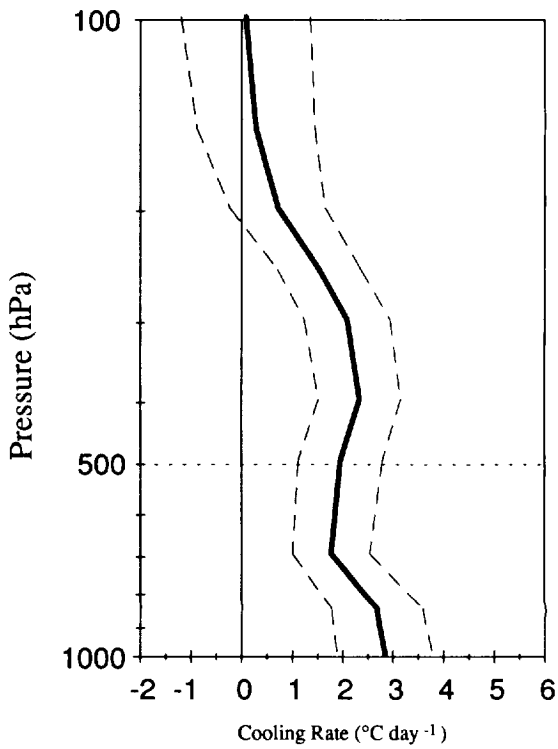

FIG. 31. As in Fig. 30 except for SE region.

The impact of upper-tropospheric water vapor was also examined. A uniform doubling of the water vapor above 500 hPa altered the longwave profiles by less than 0.5°C day^{-1} in the area that was modified. More recent ECMWF analyses altered monthly mean longwave profiles by less than this amount. The usefulness of estimating the local monthly mean by a domain-scale monthly mean was examined. Differences were found to be 0.5°C day^{-1} in the midtroposphere to 1°C day^{-1} in the lower troposphere, both at the 95% confidence level. Using a long-term mean at a point to represent an instantaneous value has similar uncertainties of 1° and 2°C day^{-1}; clouds were found to account for approximately one-half of this amount. Thus, one probably should not use a regional mean to represent the profile at a grid point, nor should a time mean be used to represent an instantaneous values at a grid point. These points should be kept in mind when applying the radiation profiles to determine convective heating profiles, as is done in our companion paper.

Acknowledgments. Our appreciation goes to Messrs. Dan Vietor and Jon Schrage for their valuable technical support. We also thank Ms. Helen Henry for typing the manuscript. The ECMWF WCRP/TOGA Archive II dataset was provided to us by NCAR, and the National Space Science Data Center assisted with the ISCCP and ERBE data. IBM provided to Purdue University the RISC-6000 workstations that were used for the bulk of the calculations. The National Center for Supercomputer Applications (NCSA) created and distributed, free of charge, the NCSA-TELNET software, which made it possible to put all of our computer resources to their best use. The National Aeronautics and Space Administration funded the majority of the research through Grant NAG8-836 and Grant NAG8-1031, issued to Dr. Dayton Vincent at Purdue University. In addition, partial support was provided by the National Science Foundation under Grant ATM-9200534, issued to Dr. Vincent at Purdue and the National Aeronautics and Space Administration Grant NAGW-3150, issued to Dr. Harshvardhan at Purdue.

REFERENCES

Ackerman, S. A., and S. K. Cox, 1987: Radiative energy budget studies for the 1979 southwest summer monsoon. *J. Atmos. Sci.*, **44,** 3052–3078.

Arakawa, A., and W. H. Schubert, 1974: Interaction of a cumulus cloud ensemble with the large-scale environment, Part I. *J. Atmos. Sci.*, **31,** 674–701.

Briglieb, B. P., 1992: Longwave band model for thermal radiation in climate studies. *J. Geophys. Res.*, **97,** 11 475–11 485.

Climate Analysis Center, 1986a: *Climate Diagnostics Bulletin.* July 1986, National Meteorological Center, NOAA/NWS, p. 1.

——, 1986b: *Climate Diagnostics Bulletin.* August 1986, National Meteorological Center, NOAA/NWS, p. 1.

Cox, S. K., and K. T. Griffith, 1979: Estimates of radiative divergence during phase III of the GARP Atlantic Tropical Experiment: Part II: Analysis of Phase III results. *J. Atmos. Sci.*, **39,** 586–601.

Darnell, W. A., W. F. Staylor, S. K. Gupta, N. A. Ritchey, and A. C. Wilber, 1992: Seasonal variation of surface radiation budget derived from International Satellite Cloud Climatology Project C1 data. *J. Geophys. Res.*, **97,** 15 741–15 760.

Dopplick, T. G., 1970: Global radiative heating of the earth's atmosphere. Rep. No. 24, Planetary Circulations Project, Dept. of Meteorology, MIT, Cambridge, MA, 128 pp.

Ellingson, R. G., J. Ellis, and S. Fels, 1991: The intercomparison of radiation codes used in climate models: Long wave results. *J. Geophys. Res.*, **96,** 8929–8953.

Gupta, S. H., 1989: A parameterization for longwave surface radiation from sun-synchronous satellite data. *J. Climate,* **2,** 305–320.

Harrison, E. F., P. Minnis, B. R. Barkstrom, V. Ramanathan, R. D. Cess, and G. G. Gibson, 1990: Seasonal variation of cloud radiative forcing derived from the Earth Radiation Budget Experiment. *J. Geophys. Res.*, **95,** 18 687–18 703.

Harshvardhan, R. Davies, D. A. Randall, and T. G. Corsetti, 1987: A fast radiation parameterization for atmospheric circulation models. *J. Geophys. Res.*, **92,** 1009–1016.

Kiehl, J. T., and B. P. Briglieb, 1992: Comparison of the observed and calculated clear sky greenhouse effect: Implications for climate studies. *J. Geophys. Res.*, **97,** 10 037–10 049.

Kuo, H. L., 1965: On formation and intensification of tropical cyclones through latent heat release by cumulus convection. *J. Atmos. Sci.*, **22,** 40–63.

——, 1974: Further studies of the parameterization of the influence of cumulus convection on large-scale flow. *J. Atmos. Sci.*, **31,** 1232–1240.

Ramsey, P. G., 1993: Radiative cooling profiles calculated from ECMWF analyses and ISCCP C1 data, and their application to determination of distributions of apparent convective heating in the equatorial Pacific. Ph.D. thesis, Dept. of Earth and Atmospheric Sciences, Purdue University, 163 pp.

Riehl, H., 1979: *Climate and Weather in the Tropics.* Academic Press, 160 pp.

Rossow, W. B., and R. A. Schiffer, 1991: ISCCP cloud data products. *Bull. Amer. Meteor. Soc.*, **72,** 2–20.

——, L. C. Garder, P.-J. Lu, and A. Walker, 1988: International Satellite Cloud Climatology Project (ISCCP) documentation of cloud data, WMO/TD-No. 266, World Meteorological Organization, Geneva, Switzerland, 78 pp. + 2 Appendices.

Schiffer, R. A., and W. B. Rossow, 1983: The International Satellite Cloud Climatology Project (ISCCP): The first project of the World Climate Research Programme. *Bull. Amer. Meteor. Soc.*, **64,** 779–784.

Slingo, A., and M. J. Webb, 1992: Simulation of clear-sky outgoing longwave radiation over the oceans using operational analyses. *Quart. J. Roy. Meteor. Soc.*, **118,** 1117–1144.

Tian, L., and J. A. Curry, 1989: Cloud overlap statistics. *J. Geophys. Res.*, **94,** 9925–9935.

Trenberth, K. E., 1992: Global analyses from ECMWF, and atlas of 1000 to 10 mb circulation statistics. NCAR/TN-373+STR, National Center for Atmospheric Research, 191 pp. + 24 fiche.

Warren, S. G., C. J. Hahn, J. London, R. M. Chervin, and R. L. Jenne, 1986: Global distribution of total cloud cover and cloud type over land. NCAR Tech. Note NCAR/TN-273+STR, National Center for Atmospheric Research, 29 pp. + 200 maps.

——, ——, ——, ——, and ——, 1988: Global distribution of total cloud cover and cloud type amounts over the ocean. NCAR/TN-317+STR, National Center for Atmospheric Research, 42 pp. + 170 maps.

Wu, M.-L. C., and C. P. Cheng, 1989: Surface downward flux computed by using geophysical parameters derived from HIRS2/MSU sounding. *Theor. Appl. Climatol.*, **40,** 37–51.

——, and J. Susskind, 1990: Outgoing longwave radiation computed by using products retrieved from HIRS2/MSU. *J. Geophys. Res.*, **95,** 7529–7602.

——, and L.-P. Chang, 1992: Longwave radiation budget parameters computed from ISCCP and HIRS2/MSU products. *J. Geophys. Res.*, **97,** 10 083–10 101.

Yanai, M., S. Esbensen, and J. H. Chu, 1973: Determination of the bulk properties of tropical cloud clusters from large-scale heat and moisture budgets. *J. Atmos. Sci.*, **30,** 611–627.